MEASUREMENTS OF MULTISTATIC X&L BAND RADAR SIGNATURES OF UAVS

Riccardo Palamà[1], Francesco Fioranelli[2], Matthew Ritchie[1], MR Inggs[3], Simon Lewis[3], Hugh Griffiths[1]

[1]Department of Electronic and Electrical Engineering, University College London, London, United Kingdom
[2]School of Engineering, University of Glasgow, Glasgow, United Kingdom
[3]Department of Electrical Engineering, University of Cape Town, Rondebosch, South Africa

***Abstract*—This paper illustrates the results of a series of measurements of multistatic radar signatures of small UAVs at L and X band. The system employed was the multistatic multiband radar system, NeXtRAD, consisting of one monostatic transmitter-receiver and two bistatic receivers. Results demonstrate the capability of the system of recording bistatic data with baselines and two-way bistatic range of the order of few kilometres.**

Keywords— multistatic radar, micro-Doppler, UAVs radar signatures

I. INTRODUCTION

The increasing presence and usage of commercially available small drones is presenting commercial opportunities (e.g. applications in filming, inspections, delivery, monitoring and surveillance), but also challenges and potential threats. Radar is one of the most promising technologies to monitor drones, as it provides operational capabilities in all weather and light conditions, with accurate estimation of range and velocities through mature range-Doppler processing.

However, drones are challenging targets for conventional radar systems, such as those installed for air traffic control. These targets are smaller (hence reduced Radar Cross Section) and more manoeuvrable than their manned counterparts or larger Unmanned Aerial Vehicles (UAVs), meaning that they can get lost in the detection of tracking process. Increasing the sensitivity of the radar would help, but the related challenge would be the significant number of false targets due to mostly birds and moving non-drone objects (vegetation, wind turbines) [1-2].

While the best radar systems and signal processing algorithms for optimal detection, tracking, and classification of drones are being actively investigated, it can be argued that access to multistatic/networked radar data can improve performances. As for other types of challenging targets, for example, small boats against intense sea clutter background, multistatic radar can benefit from multi-perspective views on the targets of interest and inherent resilience in case the target is occluded or the data degraded at one of its nodes. The majority of research available in the open literature on the radar signature of drones assumes monostatic geometries, with limited analysis of multistatic experimental drone data performed in some of the authors' previous work [3-5]. These used the NetRAD system, the S-band pulse-Doppler radar developed in collaboration between UCL and the University of Cape Town, made of three separate but identical nodes [6].

In this paper, we present initial results of an experimental campaign involving the successor of the NetRAD system, called NeXtRAD, which is capable of operating in dual-band configuration (L and X band), collecting polarimetric data at L and X-band, and operating in multistatic geometries across baselines of the order of hundreds of metres, thanks to GPS-Disciplined Oscillators (GPSDOs) [7-9].

The remainder of this paper is organised as follows. Section II presents the properties of the NeXtRAD system and addresses the data collection, Section III illustrates the preliminary results obtained, in terms of Range-Time-Intensity maps and spectrograms. Final remarks are drawn in Section IV.

II. THE NEXTRAD RADAR SYSTEM AND DATA COLLECTION

As shown in Fig. 1, NeXtRAD is made of three different nodes interconnected by a wireless network and operated by a master interface from the CnC computer ("Command & Control"). The CnC node is able to access all the local computers at each radar node ("node controllers"), but at the same time they also allow local operators access for quality control during data collection and experiments. Each node is equipped with GPSDOs to establish and maintain time and phase coherency during operations, which is fundamental for collecting valuable bistatic data. IP cameras are also mounted at the antenna pedestal for each node to allow video recordings of targets and close environment.

One of the nodes, depicted in the middle in Fig. 1, is the designated transceiver equipped with high power amplifiers (peak power 400 W at X-band and 1.6 kW at L-band) and frequency-tunable waveform generator. The typical operating frequencies are 8.5 GHz at X-band and 1.3 GHz at L-band, with bandwidths of 50 MHz. The additional two radar nodes are used as passive, receive-only nodes. Each receiver can simultaneously collect both polarimetric V and H X-band channels, meaning that full polarimetric data can be captured using alternating pulses or with two consecutive measurements using different transmitted polarisation. At L-band, where Doppler ambiguity requirements are less stringent, only one receiver chain is present, meaning that four measurements would be needed to collect complete polarisation data. At this stage, accounting for the very high cost of fast switches operating at such high transmitted power, changes in transmitted polarisation are done with manual switches.

The system is operated through a unified interface where the operators can set specified parameters (carrier frequency, pulse length, Pulse Repetition Frequency PRF, number of pulses, polarisations), which are then shared over the networks to all radar nodes. Data and metadata (the header file with the aforementioned parameters, as well as videos for ground-truth) are then stored as HDF5 files for further processing.

A. *Measurement Setup*

In this paper we report some preliminary results where the system was operated over relatively long baselines in the range of hundreds of meters. These were collected over a couple of weeks of experimental campaign performed in December 2018, in Simon's Town, with the collaboration of academic partners (UCT, UCL, University of Glasgow) and Norwegian FFI.

Fig. 2 shows a map with key locations around the area of Simon's Town and False Bay. The monostatic transceiver (yellow arrow) was located on the outdoor terrace at of a building (with antennas on the pedestal shown in Fig. 3). The bistatic nodes were located at different positions during the trials, but the most notable ones are shown by the red arrows (the closest one at Lower North, about 2.7 km from the transceiver, and the furthest one at Else Bay, about 4 km from the transceiver). The green circle on the right-hand side represents the location of a lighthouse, Roman Rock, which is located at approximately 1.8 km from the transceiver and that was often used as reference targets for range calibration and antenna alignment.

The measurement campaign involved the collection of radar returns from a hexacopter (DJI Matrice, Fig.4) and a quadcopter (DJI Phantom), flying over the sea surface at a maximum distance of about 500 m from the monostatic transceiver. The UAVs were equipped with a GPS logger device, which collected the latitude and longitude of the object with a sampling interval of about 0.2 s. Fig.5 shows an example of the plots of the monostatic range (i.e the distance between the target and the monostatic transceiver), of the two-way bistatic range (i.e. the sum of the monostatic range plus the distance between the target and the bistatic receiver located at Lower North), and the bistatic angle. We observe that during an interval of 20 s, the target covers about 30 metres along the monostatic range (from 410 m to 440 m) and 40 metres along the bistatic range (from 3090 m to 3135 m). The values of the bistatic angle are included between 87.5° and 90°. It can be noted that the bistatic angle is inversely related to the one of the bistatic range, since increasing (or decreasing) values of the bistatic range give decreasing (or increasing) values of the bistatic angle (β).

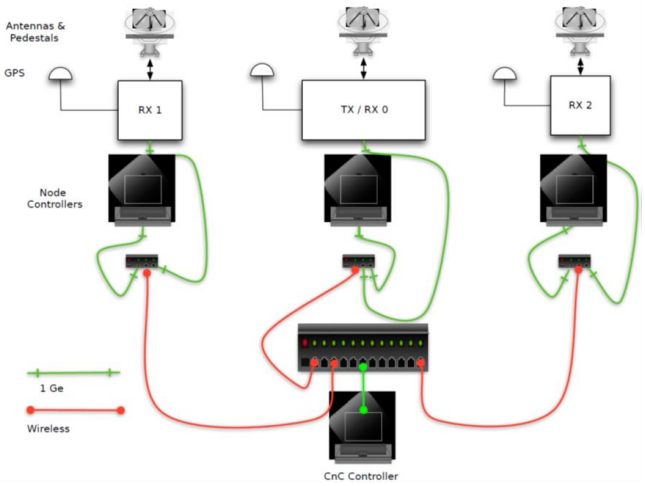

Fig.1 - Simple schematics of the NeXtRAD system, with one active transceiver (middle) and two passive receivers (left and right). The wired and wireless connections between radar nodes and controlling computers are also shown

Fig.2 - Location map of the experimental campaign performed in December 2018 near Simon's Town, South Africa. The yellow arrow corresponds to the position of the monostatic transceiver; red arrows show the position of the two bistatic receivers (Lower North, LN, the closest one, and Elsie Bay, EB, the furthest one); the green circle corresponds to the position of a lighthouse, Roman Rock RR, used as a reference target.

Fig.3- Antennas on pedestals at the location of the monostatic transceiver radar node

Fig.4 – Photograph of the hexacopter drone, DJI Matrice, in hovering position.

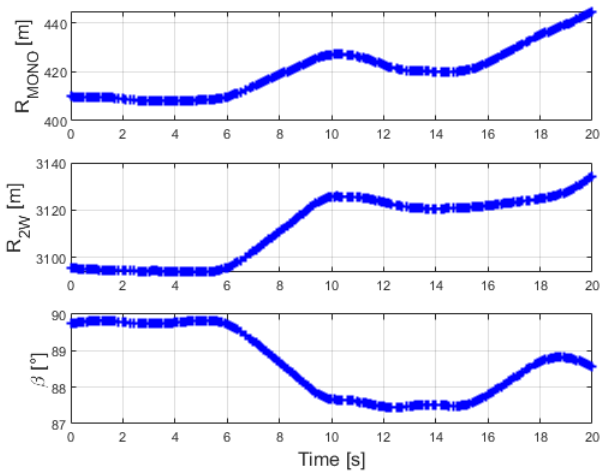

Fig.5 – Plots of the monostatic range, two-way bistatic range and bistatic angle as a function of time, extracted by the GPS logger mounted on the hexacopter. Dataset collected on the 14th Dec 2018, 10-35-43.

III. EXPERIMENTAL RESULTS

This section presents the first results obtained by analysing the data collected in the measurement campaign performed in Simon's Town, South Africa, in the first two weeks of December 2018. Fig.6 shows the normalized Range-Time-Intensity (RTI) maps of radar signatures of the hexacopter, for X band and HH polarization (i.e. both the transmitter and receiver antennas were horizontally polarized). The monostatic RTIs (Fig.6a) show a higher signal-to-noise-ratio (SNR) with respect to the bistatic RTIs (Fig.6b). Typical values of the monostatic SNR are included between 10 dB and 13 dB, whereas the bistatic SNR fluctuates between 7 dB and 10 dB. The bistatic RTIs show the presence of scatterers different from the UAV between 30 s and 50 s. A possible source of these radar returns are the birds (sea-gulls) that were flying around the drone. The GPS tracks of the hexacopter were extracted and are plotted in Fig.6 (a) and (b), superimposed on the radar data.

The drone micro-Doppler signatures were extracted using the Short Time Fourier Transform (STFT), with a moving window of 200 temporal samples, corresponding to 200 ms, with a 50% overlap, and a number of frequency samples equal to 1024. We observe that the monostatic and bistatic micro-Doppler signatures of the hexacopter at X band (Fig.7) show a slightly different behaviour. The scattering from the blades is more evident in the monostatic data, especially at HH polarization. In Fig.8 we compare the monostatic and bistatic micro-Doppler signatures of the hexacopter at L band and HH polarization. During the selected time interval (shorter than the one used for the X band data), the drone was hovering, thus its bulk yields a strong stationary component at zero Doppler. We note the presence of strong micro-Doppler returns extended within the whole spectral interval, i.e. between -500 Hz and 500 Hz. These micro-Doppler signatures are not time-stationary, as their intensity changes with time, which is probably due to small variations of the pitch and roll angles of the drone. For instance, we observe an increase of the intensity between 2.3 s and 3.3 s, for both monostatic and bistatic data.

IV. CONCLUSIONS AND FUTURE WORK

This abstract has addressed the capabilities of the multistatic multiband radar network, NeXtRAD, in measuring the radar signatures of small UAVs at large baselines, bistatic angles and bistatic ranges, for both X and L bands.

The final version of this paper will include a more exhaustive analysis of the micro-Doppler signatures of the UAVS, by using metrics such as the Doppler centroid and bandwidth. In addition, the radar signatures will be matched with the data collected by the GPS logger mounted on the UAVs (latitude, longitude, measured speed, pitch and roll angles), in order to extract common trends and behaviours. Future works will involve the use of more advanced spectral analysis tools, such as different time-frequency distributions and the wavelet transform. Detection, tracking and classification techniques will be employed to separate the UAV returns from those coming from other scatterers, such as birds and boats, exploiting the diversity yielded by using a multistatic geometry and different carrier frequencies and polarizations [10][11].

ACKNOWLEDGMENT

The authors would like to thank Adrian Stevens, Bradley Kahn, Dane Du Plessis, Darryn Jordan, Jacques Cilliers, Randy Cheng, Shirley Coetzee, Stephan Sandenbergh, Terje Johnsen, William Miceli for the support provided during the measurement campaign, and the Office of Naval Research Global, the Institution of Engineering and Technology, FFI and SA National Defence Force for the funding provided.

REFERENCES

[1] Patel, J., Fioranelli, F., Anderson, D.; 'Review of radar classification and RCS characterisation techniques for small UAVs or drones', IET Radar, Sonar & Navigation, vol. 12, no. 9, pp. 911-919, August 2018.

[2] Rahman, S., Robertson, D. A., "Radar micro-Doppler signatures of drones and birds at K-band and W-band", Nature Scientific Reports, vol. 8, 17396, (2018).

[3] Fioranelli, F., Ritchie, M., Borrion, H., Griffiths, H.; 'Classification of loaded/unloaded micro-Drones using multistatic radar', *Electronics Letters*, vol. 51, no. 22, pp. 1813-1815, October 2015.

[4] Ritchie, M., Fioranelli, F., Griffiths, H., Torvik, B.; 'Monostatic and bistatic radar measurements of birds and micro-drone', presented at *2016 IEEE Radar Conference* in May 2016, Philadelphia, PA.

[5] Hoffmann, F., Ritchie, M., Fioranelli, F., Charlish, A., Griffiths, H.; 'Micro-Doppler based detection and tracking of UAVs with multistatic radar', presented at *2016 IEEE Radar Conference* in May 2016, Philadelphia, PA

[6] T. E. Derham, S. Doughty, K. Woodbridge, C. J. Baker, 'Design and evaluation of a low-cost multistatic netted radar system', IET Radar, Sonar & Navigation, vol. 1, pp. 362-368, 2007.

[7] M. Inggs, H. Griffiths, F. Fioranelli, M. Ritchie and K. Woodbridge, "Multistatic radar: System requirements and experimental validation," 2014 International Radar Conference, Lille, 2014, pp. 1-6.

[8] S. Alhuwaimel et al., "First measurements with NeXtRAD, a polarimetric X/L Band radar network," 2017 IEEE Radar Conference (RadarConf), Seattle, WA, 2017, pp. 1663-1668.

[9] J. Sandenbergh and M. Inggs, "Synchronizing network radar using all-in-view GPS-disciplined oscillators," 2017 IEEE Radar Conference (RadarConf), Seattle, WA, 2017, pp. 1640-1645.

[10] R. Palamà, M. Greco, and F. Gini, "Multistatic adaptive CFAR detection in non-Gaussian clutter" EURASIP Journal on Advances in Signal Processing, vol. 2016, no. 107, 2016.

[11] Griffiths, H.D. and Palamà, R., 'Clutter Diversity', Chapter 6 in *Novel Radar Techniques and Applications*, Vol.2, (Klemm, R., Gierull, C., Griffiths, H.D., Lombardo, P. Koch, W. and Nickel, U. (eds)),IET, Stevenage, October 2017

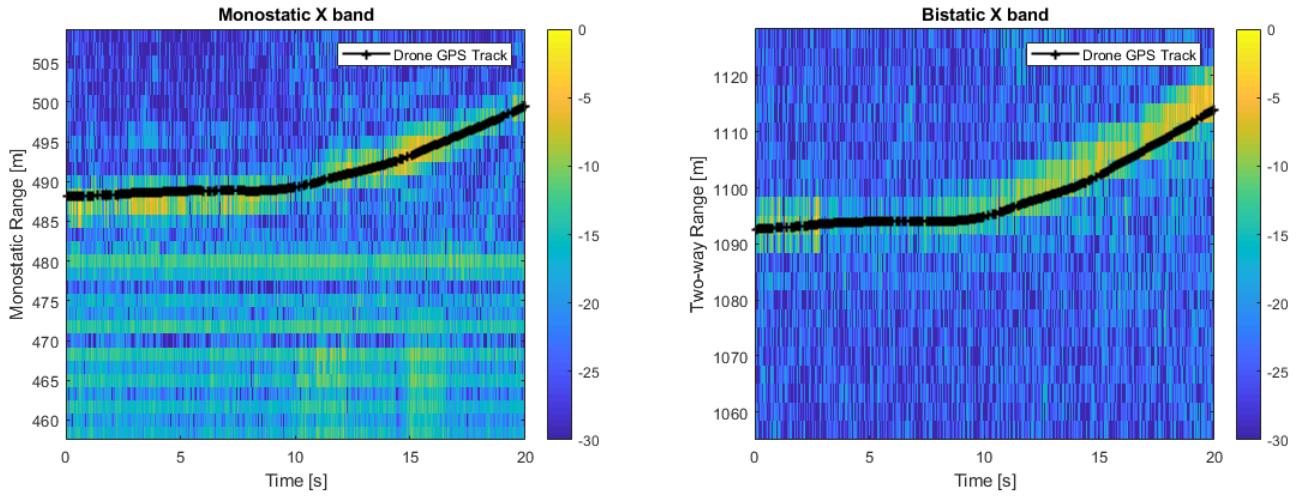

(a) (b)

Fig.6 – Range-Time-Intensity maps of the monostatic (a) and short-baseline bistatic (b) X band returns of the hexacopter at horizontal polarization (HH).

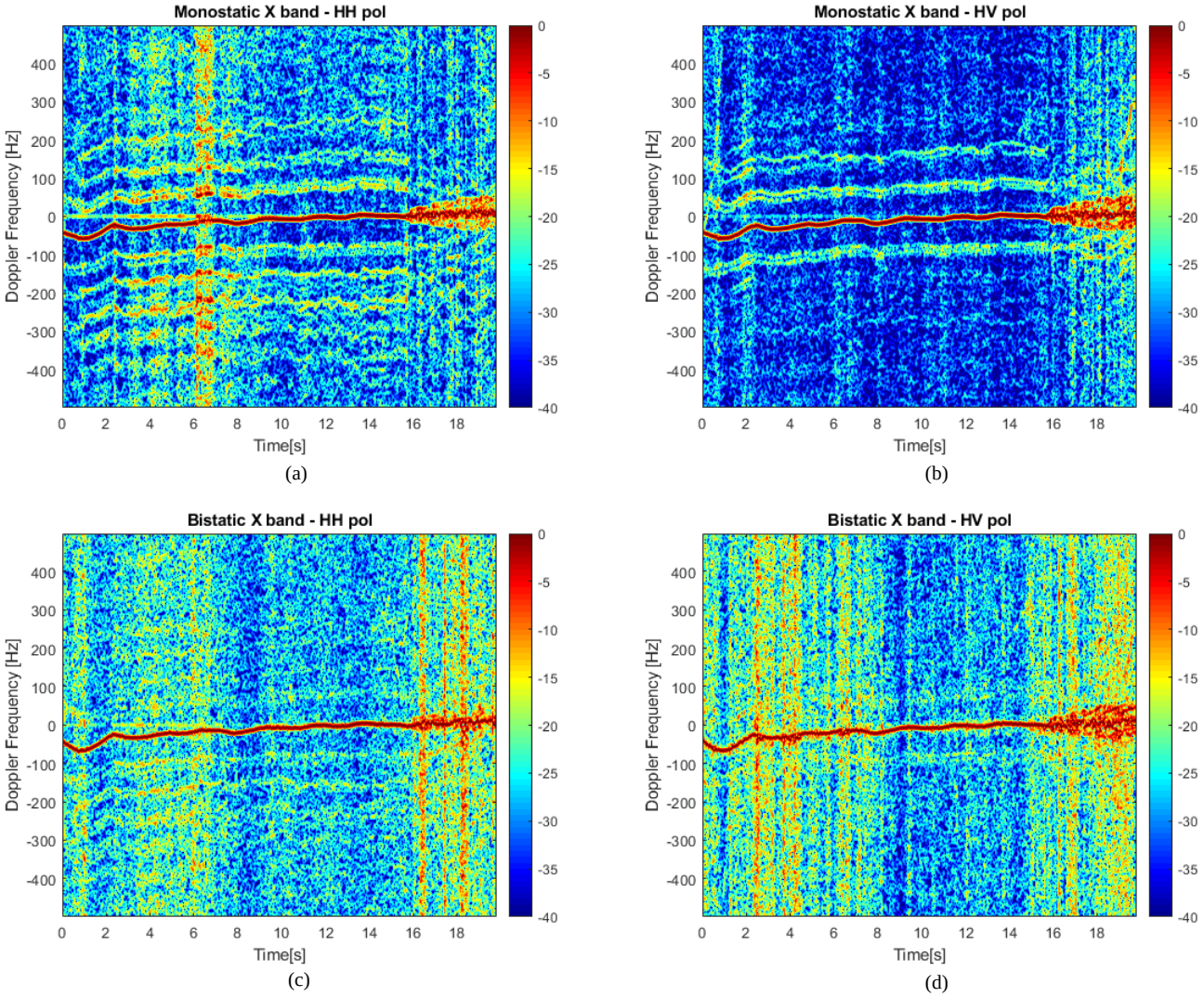

(a) (b)

(c) (d)

Fig.7 – Normalized spectrograms of X band monostatic and short-baseline bistatic signatures of the hexacopter at horizontal polarization. Monostatic VV pol (a) and VH (c), bistatic VV (b) and VH (d).

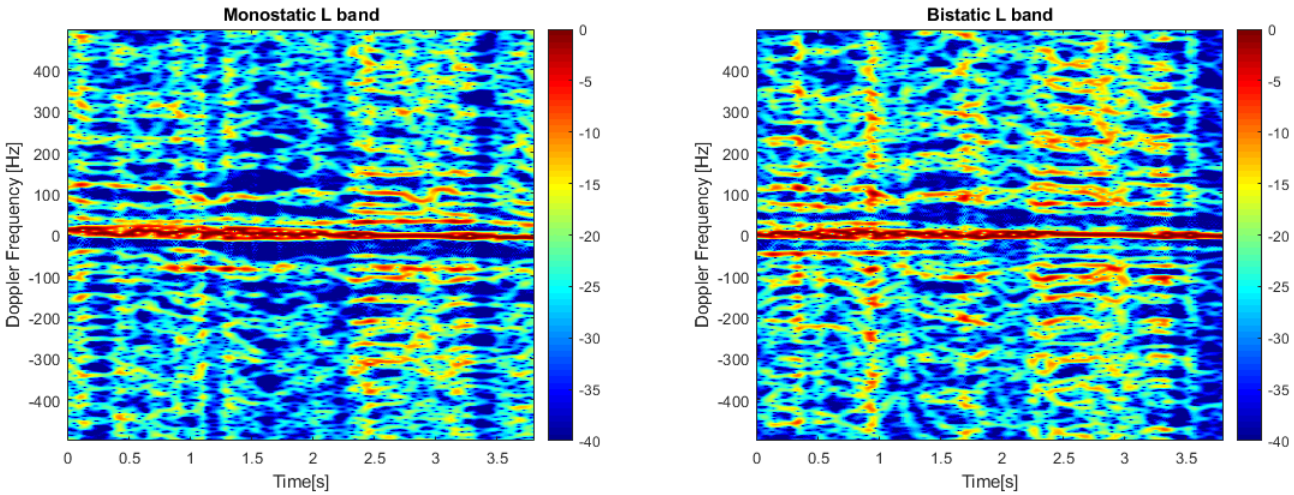

(a) (b)

Fig.8 – Normalized spectrograms of L band monostatic (a) and bistatic (b) radar signatures from the hexacopter. Data collected on 14th December 2018, bistatic baseline of 2.7 km, bistatic angle of about 90°.